


2013

# Multipole Field Effects for the Superconducting Parallel-Bar/RF-Dipole Deflecting/Crabbing Cavities

S. U. De Silva  
*Old Dominion University*

J. R. Delayen  
*Old Dominion University*

Follow this and additional works at: [https://digitalcommons.odu.edu/physics\\_fac\\_pubs](https://digitalcommons.odu.edu/physics_fac_pubs)

 Part of the [Engineering Physics Commons](#), and the [Plasma and Beam Physics Commons](#)

---

## Repository Citation

De Silva, S. U. and Delayen, J. R., "Multipole Field Effects for the Superconducting Parallel-Bar/RF-Dipole Deflecting/Crabbing Cavities" (2013). *Physics Faculty Publications*. 292.  
[https://digitalcommons.odu.edu/physics\\_fac\\_pubs/292](https://digitalcommons.odu.edu/physics_fac_pubs/292)

## Original Publication Citation

De Silva, S., & Delayen, J. (2013). *Multipole field effects for the superconducting parallel-bar/rf-dipole deflecting/crabbing cavities*. Paper presented at the 26th International Linear Accelerator Conference, Tel Aviv, Israel.

# MULTIPOLE FIELD EFFECTS FOR THE SUPERCONDUCTING PARALLEL-BAR/RF-DIPOLE DEFLECTING/CRABBING CAVITIES\*

S. U. De Silva<sup>1,2#</sup>, J. R. Delayen<sup>1,2</sup>,

<sup>1</sup>Center for Accelerator Science, Old Dominion University, Norfolk, VA 23529, USA.

<sup>2</sup>Thomas Jefferson National Accelerator Facility, Newport News, VA 23606, USA.

## Abstract

The superconducting parallel-bar deflecting/crabbng cavity is currently being considered as one of the design options in rf separation for the Jefferson Lab 12 GeV upgrade and for the crabbng cavity for the proposed LHC luminosity upgrade. The knowledge of multipole field effects is important for accurate beam dynamics study of rf structures. The multipole components can be accurately determined numerically using the electromagnetic surface field data in the rf structure. This paper discusses the detailed analysis of those components for the fundamental deflecting/crabbng mode and higher order modes in the parallel-bar deflecting/crabbng cavity.

## INTRODUCTION

The parallel-bar/RF-dipole deflecting/crabbng cavity has been optimized from a rectangular-shaped design with cylindrical-shaped parallel bars into a design with a cylindrical-shaped outer conductor with trapezoidal-shaped parallel bars [1,2], named the rf-dipole cavity. The improved rf-dipole deflecting/crabbng cavity design operating in TE<sub>11</sub>-like mode has attractive properties with low and balanced surface fields, high shunt impedance and well separated higher order modes (HOMs). The deflecting/crabbng mode is the lowest mode in the rf-dipole design.

Currently the rf-dipole design is being considered as one of the rf separator options for the Jefferson Lab 12 GeV upgrade and as one of the crabbng cavity options for proposed LHC luminosity upgrade operating at 499 MHz and 400 MHz respectively. A 750 MHz design is also being considered as a crabbng cavity for the proposed medium energy electron-ion collider (MEIC) at Jefferson Lab [3]. The first prototypes of the cylindrical-shaped 499 MHz and 400 MHz rf-dipole cavities (Fig. 1 (A) and (B)) are being fabricated and are in preparation for rf testing [4].

The 400 MHz crabbng cavity design was further modified into a square-shaped outer conductor (Fig. 1(C)) with fixed transverse dimensions of <295 mm, to meet the dimensional constraints of the LHC crabbng system. The design was further improved by curving the bar geometry at the beam aperture (Fig. 1(D)) to reduce the transverse field variation across the beam aperture.

\*Authored by Jefferson Science Associates, LLC under U.S. DOE Contract No. DE-AC05-06OR23177. The U.S. Government retains a non-exclusive, paid-up, irrevocable, world-wide license to publish or reproduce this manuscript for U.S. Government purposes.

Part of this work was done in collaboration with and supported by Niowave Inc. under the DOE STTR program.

#sdesilva@jlab.org

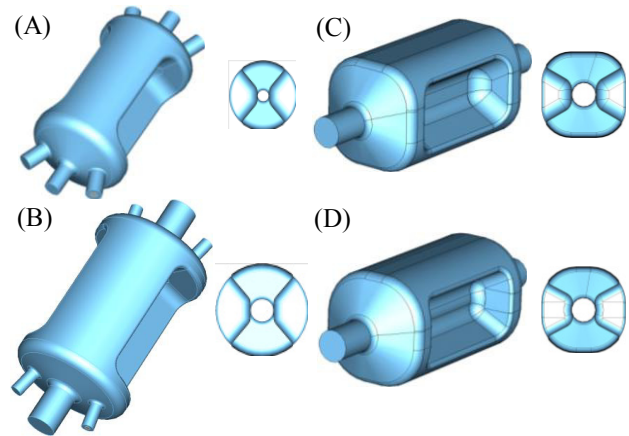


Figure 1: RF-dipole geometries and cross sections of (A) 499 MHz design, (B) cylindrical-shaped 400 MHz design, (C) square-shaped 400 MHz design and (D) square-shaped 400 MHz design with curved inner bar surfaces.

## MULTIPOLE FIELD ANALYSIS

In the rf-dipole design, the field varies across the beam aperture off the beam axis generating a non-uniform transverse deflection. The field variation in x and y directions are shown in Fig. 2, for all the rf-dipole designs mentioned in Fig. 1.

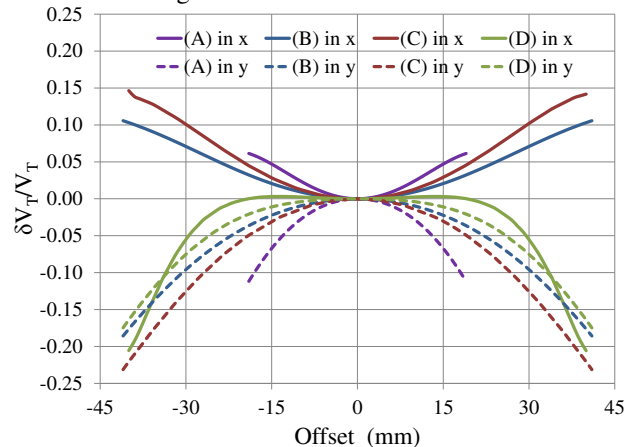


Figure 2: Normalized transverse voltage in x and y directions for designs (A), (B), (C) and (D) in Fig. 1.

The non-uniform transverse fields can generate higher orders of transverse momentum apart from the first order transverse momentum that corresponds to the deflecting or crabbng voltage. These higher order transverse multipole components may lead to perturbations in the beam. This paper presents the higher order multipole components present in the rf-dipole cavity and suppressing of those components by modifying the geometry.

04 Extreme Beams, Sources and Other Technologies

4D Beam Dynamics, Computer Simulation, Beam Transport

### Calculation of Multipole Components

The fields in magnets are often expressed in terms of multipole components. The standard representation of multipole fields [5] can be expressed as,

$$B(r, \phi) = B_{\text{ref}} \sum_{n=1}^{\infty} a_n + ib_n \left( \frac{r}{r_{\text{ref}}} \right)^{n-1} e^{i(n-1)\phi} \quad (1)$$

where  $B_{\text{ref}}$  is the reference magnetic field at a given radius of  $r_{\text{ref}}$ .

Similarly, close to the beam axis, the electro-magnetic fields in an rf cavity within the beam aperture can be represented as given in Eq. 2. The symmetry in the rf-dipole cavities doesn't produce any skew components; therefore the fields can be represented as in Eq. 3.

$$E_z(r, \phi, z) = \sum_{n=0}^{\infty} E_z^{(n)}(z) r^n e^{in\phi} \quad (2)$$

$$E_z(r, \phi, z) = \sum_{n=0}^{\infty} E_z^{(n)}(z) r^n \cos(n\phi) \quad (3)$$

The multipole field components  $E_z^{(n)}(z)$  along the beam line can be obtained by using the Fourier series expansion of  $E_z(r, \phi, z)$  as shown in Eq. 4.

$$E_z^{(n)}(z) = \frac{1}{r^n} \int_0^{2\pi} E_z(r, \phi, z) \cos(n\phi) d\phi \quad (4)$$

In rf cavities with time dependent rf fields, the higher order multipole components with time dependence can be given by  $E_{\text{acc}}^{(n)}(z) = E_z^{(n)}(z) e^{j\omega t}$ .

The higher order multipole components can be determined using the method given by A. Grudiev in Ref. [6]. The transverse momentum imparted by the higher order multipole field components ( $n > 0$ ) can be determined using the Panofsky Wenzel Theorem,

$$\begin{aligned} p_t^{(n)}(z) &= \frac{1}{c} r^{n-1} \int_{-\infty}^{\infty} F_t^{(n)} dz = -j \frac{q}{\omega} \int_{-\infty}^{\infty} \nabla_t E_z^{(n)}(z) e^{j\omega t} dz \\ &= -j \frac{q}{\omega} n r^{n-1} \int_{-\infty}^{\infty} E_{\text{acc}}^{(n)}(z) dz \end{aligned} \quad (5)$$

or by using the Lorentz Force,

$$\begin{aligned} p_t^{(n)}(z) &= \frac{1}{c} r^{n-1} \int_{-\infty}^{\infty} F_t^{(n)} dz \\ &= \frac{q}{c} r^{n-1} \int_{-\infty}^{\infty} [E_t^{(n)}(z) e^{j\omega t} + c B_t^{(n)}(z) e^{j\omega t}] dz \end{aligned} \quad (6)$$

The multipole components ( $b_n$ ) are defined using the standard definition for magnets [6] as,

$$\begin{aligned} B^{(n)}(z) &= \frac{1}{qc} F_t^{(n)}(z) = j \frac{n}{\omega} E_{\text{acc}}^{(n)}(z) \left[ \text{T/m}^{n-1} \right] \\ b_n &= \int_{-\infty}^{\infty} B^{(n)}(z) dz \left[ \text{T/m}^{n-2} \right] \end{aligned} \quad (7)$$

These coefficients ( $b_n$ ) can be used to determine the effect of higher order multipole components on beam perturbations [6].

### Multipole Components for the RF-Dipole Cavity

The rf-dipole cavity has zero on axis longitudinal electric field, where the transverse deflection is given by both transverse electric and magnetic fields. The higher order multipole components can be determined using both the methods given in Eqs. 5 and 6. The  $E_z(r, \phi, z)$  field data are obtained for each rf-dipole geometry using CST Microwave Studio, at three different radii within the beam aperture. A finer mesh as shown in Fig. 3 is used especially at smaller radii with a fixed number of points at each concentric cylinder.

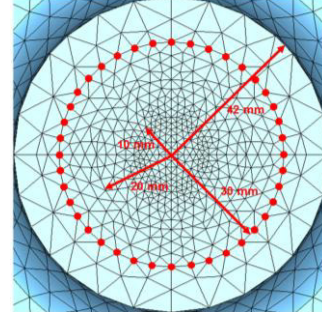


Figure 3:  $E_z^{(n)}(z)$  of  $n = 1, 3$  and  $5$  at  $r_0 = 1$  cm,  $2$  cm and  $3$  cm for the cylindrical-shaped 400 MHz rf-dipole cavity.

The Fourier-decomposed field components of  $E_z^{(n)}(z)$ ,  $E_x^{(n)}(z)$  and  $H_y^{(n)}(z)$  calculated using a MatLAB code at radii of  $1$  cm,  $2$  cm and  $3$  cm normalized to a transverse voltage (V) of  $1$  V are shown in Fig. 4, 5 and 6 for the cylindrical-shaped 400 MHz crabbing cavity. At radii closer to the beam axis the field data has higher noise content. Also, as the order increases, the noise content increases and becomes dominant over the field content. The rf-dipole cavity has components of order  $2n$  for  $n = 1, 2, 3$ , etc. In the rf-dipole cavity the  $E_z^{(n)}(z) \sin(\omega t)$  components corresponds to that of deflecting cavities and  $E_z^{(n)}(z) \cos(\omega t)$  corresponds to the components related to crabbing cavities with a synchronous phase of  $\phi_s = 90^\circ$ . The higher order multipole components ( $b_n$ ) can be determined by either using the Panofsky-Wenzel Theorem (Eq. 5) or using Lorentz Force (Eq. 6).

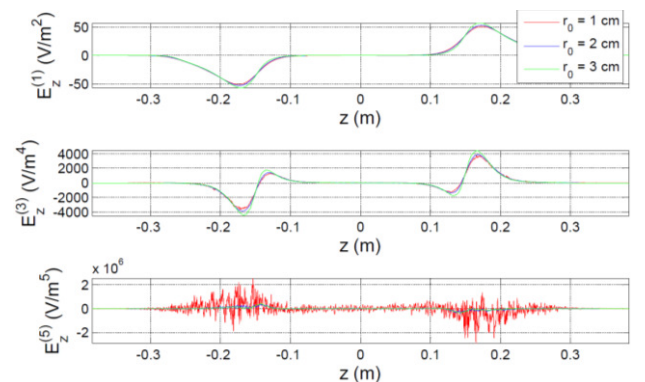


Figure 4:  $E_z^{(n)}(z)$  of  $n = 1, 3$  and  $5$  at  $r_0 = 1$  cm,  $2$  cm and  $3$  cm for the cylindrical-shaped 400 MHz rf-dipole cavity.

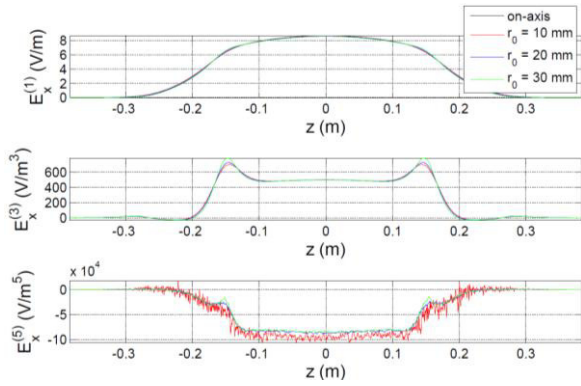


Figure 5:  $E_x^{(n)}(z)$  of  $n = 1, 3$  and  $5$  at  $r_0 = 1$  cm,  $2$  cm and  $3$  cm for the cylindrical-shaped 400 MHz rf-dipole cavity.

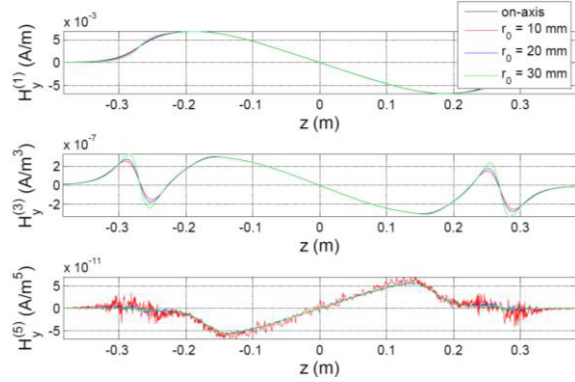


Figure 6:  $H_y^{(n)}(z)$  of  $n = 1, 3$  and  $5$  at  $r_0 = 1$  cm,  $2$  cm and  $3$  cm for the cylindrical-shaped 400 MHz rf-dipole cavity.

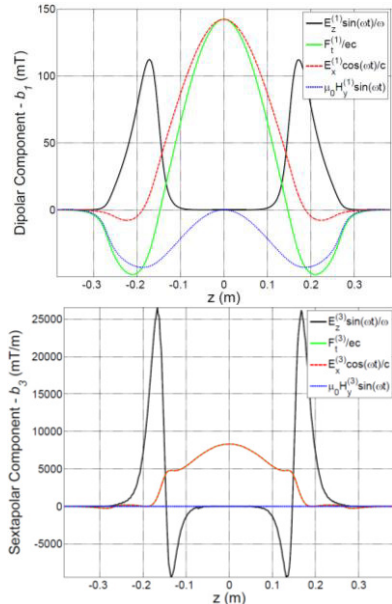


Figure 7: Dipolar and sextapolar field components of the 400 MHz cylindrical-shaped rf-dipole cavity.

The field components of the first two non-zero multipole components are shown in Fig. 7. The components  $F_t^{(1)}/c$  and  $E_{acc}^{(1)}(z)/\omega = E_z^{(n)}(z)\sin(\omega t)/\omega$  has different dependence on  $z$ , however gives the same  $b_1$  when integrated along  $z$ , that corresponds to the transverse voltage given by the rf-dipole cavity.

The higher order multipole components of the fundamental deflecting/crabbing mode are shown in Table 1, for the four rf-dipole designs shown in Fig. 1. As seen by the field profiles the  $b_n$  for  $n = 0, 2, 4, 6, \dots$  are zero. All the higher order multipole components are normalized to a transverse voltage ( $V_t$ ) of 1.0 MV. Comparing the 400 MHz crabbing cavities of cylindrical-shaped outer conductor, the 400 MHz cavity with a square shaped outer conductor has higher multipole components. The square-shaped 400 MHz rf-dipole cavity with curved bar surfaces has reduced  $b_3$  and  $b_5$ , but has higher  $b_7$  compared to the other 400 MHz designs.

Table 1: Multipole components for the rf-dipole cavity designs shown in Fig. 1.

	(A)	(B)	(C)	(D)	Units
$V_z$	0.0	0.0	0.0	0.0	MV
$V_t$	1.0	1.0	1.0	1.0	MV
$b_1$	3.3	3.3	3.3	3.3	mT m
$b_2$	0.0	0.0	0.0	0.0	mT
$b_3$	$8.3 \times 10^2$	$3.0 \times 10^2$	$4.1 \times 10^2$	$1.0 \times 10^2$	mT/m
$b_4$	0.0	0.0	0.0	0.0	mT/m <sup>2</sup>
$b_5$	$-5.8 \times 10^5$	$-4.6 \times 10^4$	$-4.1 \times 10^4$	$-2.2 \times 10^4$	mT/m <sup>3</sup>
$b_6$	0.0	0.0	0.0	0.0	mT/m <sup>4</sup>
$b_7$	$-7.1 \times 10^8$	$-1.03 \times 10^7$	$-2.0 \times 10^7$	$-6.9 \times 10^7$	mT/m <sup>5</sup>

## CONCLUSION

The higher order multipole components were calculated for the rf-dipole cavity designs of different geometries. The modified square-shaped 400 MHz cavity with curved bar surfaces has improved lower order multipole components. The values of the multipole components are comparable to standard magnets in a beam line. The rf-dipole geometry requires further optimization in suppressing the dominant multipole components, and therefore needs to be considered as a design optimization parameter.

## REFERENCES

- [1] J.R. Delayen and S.U. De Silva, in Proceedings of the 15<sup>th</sup> International Conference on RF Superconductivity, Chicago, Illinois (2011), p. 219.
- [2] S.U. De Silva and J.R. Delayen, in Proceedings of the 15<sup>th</sup> International Conference on RF Superconductivity, Chicago, Illinois (2011), p. 135.
- [3] A. Castilla et.al., in Proceedings of the 3<sup>rd</sup> International Particle Accelerator Conference, New Orleans, Louisiana (2012), p. 2447.
- [4] S.U. De Silva and J.R. Delayen, in Proceedings of the 3<sup>rd</sup> International Particle Accelerator Conference, New Orleans, Louisiana (2012), p. 2453.
- [5] A.W. Chao and M. Tigner, "Handbook of Accelerator Physics and Engineering", (World Scientific Publishing Co. Pte. Ltd), 1999.
- [6] J. Barranco Garcíaorelov et.al., in Proceedings of the 3<sup>rd</sup> International Particle Accelerator Conference, New Orleans, Louisiana (2012), p. 1873.